Thin Dielectric Sheet Simulation by Surface Integral Equation Using Modified RWG and Pulse Bases

I-Ting Chiang, *Member, IEEE*, and Weng Cho Chew, *Fellow, IEEE*

***Abstract*—The conventional thin dielectric sheet surface integral equation, proposed by Harrington and Mautz, is reviewed. Due to its simplicity and inadequency for certain problems, a new surface integral equation is proposed to fill the gap. This new formulation takes both tangential and normal currents into account so that it can handle problems with high and low permittivity and grazing incident waves. Based on the D-field formulation, inhomogeneity and surface charge can be treated correctly. Modelling the geometry by triangles, this surface integral equation is discretized and is suitable for the method of moments to solve. Rao–Wilson–Glisson and pulse functions are employed simultaneously for basis and testing functions and so the moment solution has full descriptions of polarization current in the thin dielectric layer. Several examples are examined by both analytical and other published numerical methods. These results show excellent agreement and demonstrate the validity and effectiveness of this new integral equation.**

***Index Terms*—Method of moments (MoM), pulse, radome, resistive sheet, Rao–Wilson–Glisson (RWG), scattering, surface integral equation (SIE), thin dielectric sheet (TDS).**

I. Introduction

FOR protection or aerodynamic reasons, an antenna or a scatterer is usually enclosed by a radome [1], which is made of dielectric layers. The presence of a radome in general affects the original radiation characteristics of an antenna such as the far-field pattern and its resonance frequency since current is induced on the radome. In addition, more and more nonmetallic structures have replaced metallic ones to reduce the weight or the radar cross section (RCS), especially in the construction of modern aircraft [2], [3]. Investigation of a thin dielectric layer sheet is thus important and has been extensively explored during the past three decades [4]–[11].

For dielectric layer problem, the volume integral equation (VIE) approach [12]–[16], solved by the method of moments (MoM) [17], is one of the popular analysis methods due to its flexibility and capability of handling arbitrary shapes and inhomogeneity. The tetrahedral model proposed in [14] is preferred over the cubic-pulse approach in [13], [15] or rooftop approach in [16] since tetrahedral meshes are conformal to geometry with curvature. In addition, this method does not introduce fictitious charge at mesh surface, which is another desirable property for numerical accuracy.

The VIE approach using tetrahedral modelling [14], however, has two disadvantages for thin dielectric layer problems. One is the difficulty in tetrahedron construction. When the thickness of the layer is very thin, the tetrahedron tends to be excessively flat and it may cause commercial automeshers to generate defective tetrahedrons (for example four nodes on a plane). Care has to be taken so that these defective tetrahedrons are corrected or removed before simulation proceeds. Even if all tetrahedrons are generated correctly, it is not guaranteed to work in MoM codes since the nodes of these tetrahedrons are usually stored in double precision after mesh construction, while the MoM codes are usually run in single precision. This format inconsistency may cause the breakdown of MoM codes or give incomplete solutions. For example, the information of normal currents are lost due to insufficient machine precision. One possible remedy to the above problem is to increase the mesh density so that no excessively flat tetrahedrons are generated and MoM codes can read it correctly in single precision. Nevertheless, it gives unnecessarily high mesh density and number of unknowns, which requires additional memory and run time. The other disadvantage is the inefficiency of tetrahedral modelling. Take a thin plate meshed with one layer of tetrahedrons for example. If there are respective N triangles on the top and bottom surfaces, it leads to about $3N$ tetrahedrons in total, which contributes to more than $6N$ unknowns. It is pertinent to point out that the two disadvantages do not only exist in the tetrahedron modelling but also exist in other volume mesh modelling such as [13], [15], [16]. The method using cubic cells is even difficult to model a curved object.

To reduce the exorbitant cost for thin dielectric layer simulation and ease the difficulty in volume mesh modelling by the VIE, the thin dielectric sheet (TDS) formulation is favored. The idea, which can be traced back to [4] in 1975, is that when the thickness of a TDS is very small compared to the wavelength, the field varies very little with respect to the normal direction. The volume integral can be approximately reduced to a surface integral and the VIE degenerates into a surface integral equation (SIE), which is easier to solve. In this way, the geometry is modelled as a surface instead of a volume. The resultant SIE can be solved by MoM using the popular RWG basis [18]. For a surface meshed with N triangles, it results in about $1.5N$ unknowns using Harrington's method in [4] or $2.5N$ unknowns by our method, which will be detailed later. Apparently, TDS SIE approach requires much simpler meshes and needs less unknowns. In addition, it is easier for meshing as well. So it is more advantageous to solve thin sheet problems by TDS SIE than by VIE.

Manuscript received August 12, 2005; revised December 29, 2005. This work is supported by the Air Force Office of Scientific Research (AFOSR) Multidisciplinary University Research Initiative (MURI) under Grant FA9550-04-1-0326.

The authors are with the Center for Computational Electromagnetics and Electromagnetics Laboratory, Department of Electrical and Computer Engineering, University of Illinois at Urbana-Champaign, Urbana, IL 61801-2991 USA (e-mail: itchiang@sunchew.ece.uiuc.edu).

Digital Object Identifier 10.1109/TAP.2006.877180

This paper is organized as follows. The conventional TDS formulation is reviewed in the next section. A new surface integral equation formulation is given in Section III. The MoM solution procedure and matrix evaluation is described in Section IV. Numerical examples are demonstrated and discussed in Section V. Last but not least, conclusions are highlighted in Section VI.

II. Review of the Conventional TDS Formulation

Consider a thin dielectric layer with thickness τ and dielectric constant $\varepsilon_r(\mathbf{r})$ as shown in Fig. 1. With the incident wave $\mathbf{E}^i(\mathbf{r})$ and the polarization current $\mathbf{J}_v(\mathbf{r})$ in the dielectric object, the VIE in the manner of [4] is described as

$$\mathbf{E}^i(\mathbf{r}) = \frac{-\mathbf{J}_v(\mathbf{r})}{i\omega\varepsilon_0\left[\varepsilon_r(\mathbf{r})-1\right]} - i\omega\mu_0\int_V \mathbf{J}_v(\mathbf{r}')g(\mathbf{r},\mathbf{r}')dV' + \frac{\nabla}{i\omega\varepsilon_0}\int_V \nabla'\cdot\mathbf{J}_v(\mathbf{r}')g(\mathbf{r},\mathbf{r}')dV' \quad (1)$$

where

$$g(\mathbf{r},\mathbf{r}') = \frac{e^{ik_o|\mathbf{r}-\mathbf{r}'|}}{4\pi|\mathbf{r}-\mathbf{r}'|} \quad (2)$$

is the 3-D Green's function. In this paper, we use $e^{-i\omega t}$ as the time harmonic factor. When the dielectric constant $\varepsilon_r(\mathbf{r})$ is large, the incident wave will almost penetrate the TDS perpendicularly and tangential fields dominate in the dielectric. Therefore, normal fields could be ignored in this situation. In addition, when the thickness τ is very small compared to the wavelength, the volume integral can be approximated as $dV' \approx \tau \times dS'$. So (1) can be written as

$$\mathbf{E}^i_{tan}(\mathbf{r}) \approx Z_s(\mathbf{r})\mathbf{J}_s(\mathbf{r}) - i\omega\mu_0\int_S \mathbf{J}_s(\mathbf{r}')g(\mathbf{r},\mathbf{r}')dS' + \frac{\nabla}{i\omega\varepsilon_0}\int_S \nabla'\cdot\mathbf{J}_s(\mathbf{r}')g(\mathbf{r},\mathbf{r}')dS' \quad (3)$$

where

$$\mathbf{J}_s(\mathbf{r}) = \tau\mathbf{J}_v(\mathbf{r}) \quad (4)$$

is the surface current to be solved for and

$$Z_s(\mathbf{r}) = \frac{i}{\omega\varepsilon_0\left[\varepsilon_r(\mathbf{r})-1\right]\tau} \quad (5)$$

is the surface impedance. Some special values of the dielectric constant $\varepsilon_r(\mathbf{r})$ and thickness τ are worthy of discussion. For $\varepsilon_r(\mathbf{r}) = 1$ or $\tau = 0$, which means that the TDS does not exist, the surface impedance $Z_s(\mathbf{r})$ is infinite and the surface current $\mathbf{J}_s(\mathbf{r})$ is zero. For $\varepsilon_r(\mathbf{r}) = \infty$, which means the TDS is a PEC, the surface impedance is zero and the resultant SIE is the same as that we commonly solve for PEC. Intuitively, large $Z_s(\mathbf{r})$ means that less surface current is induced and less electromagnetic field is scattered. Small $Z_s(\mathbf{r})$ means the dielectric is rather conductive and the TDS behaves toward a PEC.

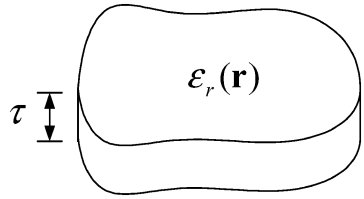

Fig. 1. Geometry of a thin dielectric sheet with thickness τ and dielectric constant $\varepsilon_r(\mathbf{r})$.

Because (3) is very similar to the SIE for PEC, we can treat (3) as a special case of PEC scattering problems. Moreover, since computer MoM codes for PEC problems are rather matured and well developed, based on previous PEC codes, hybrid PEC-TDS codes can be programmed easily. For example, the proposed RWG basis for PEC problems in [18] can be employed to solve TDS problems as well. Although this strategy is attractive and successful in many situations, some problems are observed and pointed out as follows.

First, (3) is not suitable for low contrast cases. In general, the smaller the dielectric constant, the larger is the ratio of the normal current to the tangential current induced in the dielectric. In practice, it is, however, difficult to anticipate if the dielectric constant is large or small. So the accuracy of the MoM solution is questionable for certain range of the dielectric constant. The second problem is that for nearly grazing incident wave, this simple TDS formulation loses its accuracy even in the high permittivity case [7]. In this case, the normal current is comparable to or even much larger than the tangential current. This formulation breaks down resulting from the negligence of the normal current. Third, the PEC-based TDS codes also cause inaccuracy due to incorrect boundary conditions at the surface edges. For PEC, the surface current flows parallel to the edge and is not allowed to flow into it. But a TDS is a dielectric and the polarization current does not have this restriction. Charge is induced at the edge as well. For certain situations, this erroneous representation of edge boundary conditions will lead to anomalies in the solution.

For the above three problems, the root of the first two is the lack of normal current in the formulation. The third stems from incorrect edge boundary conditions. To remedy these problems, a more complete formulation will be derived in the next section.

III. New TDS Surface Integral Formulation

As pointed out in [14], VIE is best described by the D-field formulation since the electric flux has a continuous normal component at media interface. Hence (1) is reformulated [19] as

$$\mathbf{E}^i(\mathbf{r}) = \frac{\mathbf{D}(\mathbf{r})}{\varepsilon_0\varepsilon_r} + \frac{k_0^2}{\varepsilon_0}\int_V \chi(\mathbf{r}')\mathbf{D}(\mathbf{r}')g(\mathbf{r},\mathbf{r}')dV' + \frac{\nabla}{\varepsilon_0}\int_V \nabla'\cdot\left[\chi(\mathbf{r}')\mathbf{D}(\mathbf{r}')\right]g(\mathbf{r},\mathbf{r}')dV' \quad (6)$$

where

$$\chi(\mathbf{r}) = \frac{1}{\varepsilon_r(\mathbf{r})} - 1. \quad (7)$$

Note that

$$\nabla \cdot \chi(\mathbf{r})\mathbf{D}(\mathbf{r}) = \nabla\chi(\mathbf{r}) \cdot \mathbf{D}(\mathbf{r}) + \chi(\mathbf{r})\nabla \cdot \mathbf{D}(\mathbf{r}) = \rho_s + \rho_v \quad (8)$$

where ρ_s is the surface charge density and ρ_v is the volume charge density. In the numerical implementation such as the tetrahedral modelling in [14] or the modified RWG basis we will mention in the next section, the material is uniform in each discretized domain and hence the term $\nabla\chi(\mathbf{r})$ in (8) introduces a delta function at the junction surface. By the theory of the generalized function, the surface charge density is evaluated as

$$\rho_s = \left[\chi^-(\mathbf{r}) - \chi^+(\mathbf{r})\right] \hat{n} \cdot \mathbf{D}(\mathbf{r}) \quad (9)$$

where $\chi^+(\mathbf{r})$ is the contrast ratio in the dielectric domain T_q^+, $\chi^-(\mathbf{r})$ is the contrast ratio in the dielectric domain T_q^-, $\hat{n}$ is the unit normal vector pointing out of T_q^+, and $\mathbf{r}$ is on the junction surface of T_q^+ and T_q^-. The volume charge density ρ_v vanishes because of the fact $\nabla \cdot \mathbf{D}(\mathbf{r}) = 0$. In addition

$$\begin{aligned} \nabla \cdot \mathbf{D}(\mathbf{r}) &= 0 = \nabla_t \cdot \mathbf{D}_t(\mathbf{r}) + \hat{n}\frac{\partial}{\partial n} \cdot \mathbf{D}_n(\mathbf{r}) \\ &\approx \nabla_t \cdot \mathbf{D}_t(\mathbf{r}) + \hat{n} \\ &\quad \cdot \frac{\mathbf{D}_n^+(\mathbf{r} \in S_n^+) - \mathbf{D}_n^-(\mathbf{r} \in S_n^-)}{\tau}. \end{aligned} \quad (10)$$

$\mathbf{D}_t(\mathbf{r})$ is the tangential component of $\mathbf{D}(\mathbf{r})$. $\mathbf{D}_n^+(\mathbf{r})$ and $\mathbf{D}_n^-(\mathbf{r})$ are the normal components of $\mathbf{D}(\mathbf{r})$ at top and bottom surfaces, respectively. By (6), (8), (9) and (10), the integral for the scalar potential term is rearranged as

$$\begin{aligned} &\int_V \nabla' \cdot [\chi(\mathbf{r}')\mathbf{D}(\mathbf{r}')]\, g(\mathbf{r},\mathbf{r}')dV' \\ &= \int_V \nabla'\chi(\mathbf{r}') \cdot \mathbf{D}(\mathbf{r}')g(\mathbf{r},\mathbf{r}')dV' \\ &= \int_{S_t} \triangle\chi_t \hat{t} \cdot \mathbf{D}_t(\mathbf{r}')g(\mathbf{r},\mathbf{r}')dS' \\ &\quad + \int_{S_n^+} \triangle\chi_n^+ \hat{n} \cdot \mathbf{D}_n^+(\mathbf{r}')g(\mathbf{r},\mathbf{r}')dS' \\ &\quad - \int_{S_n^-} \triangle\chi_n^- \hat{n} \cdot \mathbf{D}_n^-(\mathbf{r}')g(\mathbf{r},\mathbf{r}')dS' \end{aligned} \quad (11)$$

where

$$\begin{cases} \triangle\chi_t = \chi^- - \chi^+, & \mathbf{r} \in S_t \\ \triangle\chi_n^+ = \chi^- - \chi^+, & \mathbf{r} \in S_n^+ \\ \triangle\chi_n^- = \chi^- - \chi^+, & \mathbf{r} \in S_n^-. \end{cases} \quad (12)$$

χ^+ and χ^- in (12) respectively denote the contrast ratio inside and outside the dielectric domain as shown in Fig. 2. The three integrals in the last line of (11) denote the contributions from the lateral, upper and lower surfaces, respectively. By (10) and (11), when $\tau \to 0$, (6) is approximated as

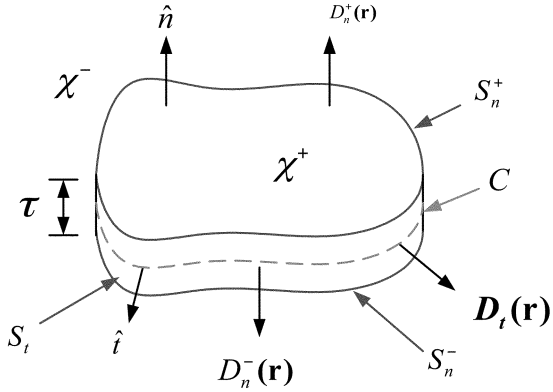

Fig. 2. A thin dielectric sheet with associated quantities.

$$\begin{aligned} \mathbf{E}^i(\mathbf{r}) \approx{}& \frac{\mathbf{D}(\mathbf{r})}{\varepsilon_0\varepsilon_r(\mathbf{r})} + \frac{k_0^2}{\varepsilon_0}\tau \int_S \chi(\mathbf{r}')\mathbf{D}(\mathbf{r}')g(\mathbf{r},\mathbf{r}')dS' \\ &+ \frac{\nabla}{\varepsilon_0}\left\{ \tau \int_C \triangle\chi_t \hat{t} \cdot \mathbf{D}_t(\mathbf{r}')g(\mathbf{r},\mathbf{r}')dl' \right. \\ &\quad - \tau \int_{S_n^-} \triangle\chi_n^- \nabla_t' \cdot \mathbf{D}_t(\mathbf{r}')g(\mathbf{r},\mathbf{r}')dS' \\ &\quad + \int_{S_n^+} \triangle\chi_n^+ \hat{n} \cdot \mathbf{D}_n^+(\mathbf{r}')g(\mathbf{r},\mathbf{r}')dS' \\ &\quad \left. - \int_{S_n^-} \triangle\chi_n^- \hat{n} \cdot \mathbf{D}_n^+(\mathbf{r}')g(\mathbf{r},\mathbf{r}')dS' \right\}. \end{aligned} \quad (13)$$

Note that the scalar potential term has four integrals in the bracket to separate the contributions from tangential and normal fields. All the quantities in (10), (11), (12), and (13) are illustrated in Fig. 2. The scalar potential term is more complex than (3) for including all surface charges. Note that $\mathbf{D}_n^+(\mathbf{r})$ is the only normal component of $\mathbf{D}(\mathbf{r})$ in (13) since $\mathbf{D}_n^-(\mathbf{r})$ has be replaced by $\nabla_t \cdot \mathbf{D}_t(\mathbf{r})$ and $\mathbf{D}_n^+(\mathbf{r})$ using (10). This new TDS integral equation includes essential physics and is ready to solve by MoM.

IV. MoM Solution

Because the electric flux in (13) is decomposed into normal and tangential parts, it can be specified by two sets of basis functions numerically. For the conforming capability of arbitrary geometrical shapes, RWG basis [18] is the most popular of all by far. The RWG basis is first developed for PEC surfaces and it is defined by a triangle pair. In this way, no charge accumulates at the PEC edges. For the TDS, we need to modify it since charge is enforced to exist at the edges between air-dielectric media. This can be worked out by defining a half basis as that in the

tetrahedral modelling for VIE in [14]. So both regular and half RWG bases, which may be called modified RWG basis, are employed for the tangential component of the electric flux. For the normal component, pulse basis is used for simplicity.

To solve (13), we let

$$\begin{aligned}\mathbf{D}(\mathbf{r}) &= \mathbf{D}_t(\mathbf{r}) + \mathbf{D}_n^+(\mathbf{r}) \\ &\cong \sum_{q=0}^{Q-1} D_q \mathbf{f}_q(\mathbf{r}) + \sum_{n=0}^{N-1} D_n \mathbf{p}_n(\mathbf{r}).\end{aligned} \tag{14}$$

Q is the number of total edges (including interior and boundary edges) and N is the number of total triangles. $\mathbf{f}_q(\mathbf{r})$ is the RWG basis defined as

$$\mathbf{f}_q(\mathbf{r}) = \begin{cases} \frac{l_q}{2A_q^+}\boldsymbol{\rho}_q^+, & \mathbf{r} \in T_q^+ \\ \frac{l_q}{2A_q^-}\boldsymbol{\rho}_q^-, & \mathbf{r} \in T_q^- \\ 0, & \text{otherwise} \end{cases} \tag{15}$$

where l_q is the length of the shared edge and $A_q^\pm$ is the area of the triangle $T_q^\pm$. For half basis, only T_q^+ is defined at the edge of an open surface. $\mathbf{p}_n(\mathbf{r})$ is the triangle pulse basis defined as

$$\mathbf{p}_n(\mathbf{r}) = \begin{cases} \hat{n}_n, & \mathbf{r} \in T_n \\ 0, & \mathbf{r} \notin T_n \end{cases} \tag{16}$$

where $\hat{n}_n$ is the unit normal vector of the triangle T_n. By Galerkin's testing procedure, a matrix equation is obtained

$$\begin{bmatrix} Z_{TT} & Z_{TN} \\ Z_{NT} & Z_{NN} \end{bmatrix} \cdot \begin{bmatrix} I_T \\ I_N \end{bmatrix} = \begin{bmatrix} V_T \\ V_N \end{bmatrix} \tag{17}$$

where Z_{TT} denotes the interaction between tangential fields, Z_{TN} and Z_{NT} denotes the interaction between tangential and normal fields, Z_{NN} denotes the interaction between normal fields, V_T denotes the excitation from incident tangential fields, and V_N denotes the excitation from incident normal fields.

The evaluations of Z_{TT}, V_T and V_N are straightforward and can be referred to [18]. The evaluation of Z_{TN} is

$$Z_{TN,pn} = -i\omega\langle \mathbf{A}_{TN,n}, \mathbf{f}_p \rangle + \langle \nabla\phi_{TN,n}, \mathbf{f}_p \rangle \tag{18}$$

where

$$\mathbf{A}_{TN,n} = \hat{n}_n \frac{i\omega\mu_o\tau\chi_n}{4\pi} \int_{T_n} \frac{e^{ik_oR}}{R} dS' \tag{19}$$

$$\boldsymbol{\phi}_{TN,n} = \frac{1}{4\pi\varepsilon_o} \left[\triangle\chi_{n,n}^+ \int_{T_n^+} \frac{e^{ik_oR}}{R} dS' - \triangle\chi_{n,n}^- \int_{T_n^-} \frac{e^{ik_oR}}{R} dS' \right] \tag{20}$$

and $R = |\mathbf{r} - \mathbf{r}'|$. The evaluation of Z_{NT} is

$$Z_{NT,mq} = -i\omega\langle \mathbf{A}_{NT,q}, \mathbf{p}_m \rangle + \langle \nabla\phi_{NT,q}, \mathbf{p}_m \rangle \tag{21}$$

where

$$\mathbf{A}_{NT,q} = \frac{i\omega\mu_o\tau l_q}{8\pi} \left[\frac{\chi_q^+}{A_q^+} \int_{T_q^+} \rho_q^+ \frac{e^{ik_oR}}{R} dS' + \frac{\chi_q^-}{A_q^-} \int_{T_q^-} \rho_q^- \frac{e^{ik_oR}}{R} dS' \right] \tag{22}$$

$$\begin{aligned}\phi_{NT,q} = &\frac{\tau}{4\pi\varepsilon_o} \\ &\times \left\{ \triangle\chi_{t,q} \int_{l_q} \frac{e^{ik_oR}}{R} dl' - l_q \frac{\triangle\chi_{n^-,q}^+}{A_q^+} \int_{T_q^+} \frac{e^{ik_oR}}{R} dS' \right. \\ &\left. q + l_q \frac{\triangle\chi_{n^-,q}^-}{A_q^-} \int_{T_q^-} \frac{e^{ik_oR}}{R} dS' \right\}.\end{aligned} \tag{23}$$

The evaluation of Z_{NN} is

$$Z_{NN,mn} = -i\omega\langle \mathbf{A}_{NN,n}, \mathbf{p}_m \rangle + \langle \nabla\phi_{NN,n}, \mathbf{p}_m \rangle \tag{24}$$

where

$$\mathbf{A}_{NN,n} = \hat{n}_n \frac{i\omega\mu_o\tau\chi_n}{4\pi} \int_{T_n} \frac{e^{ik_oR}}{R} dS' \tag{25}$$

$$\phi_{NN,n} = \frac{1}{4\pi\varepsilon_o} \left[\triangle\chi_{n,n}^+ \int_{T_n^+} \frac{e^{ik_oR}}{R} dS' - \triangle\chi_{n,n}^- \int_{T_n^-} \frac{e^{ik_oR}}{R} dS' \right]. \tag{26}$$

After all these matrix elements have been evaluated, I_T and I_N can be solved by direct or iterative matrix solvers.

V. Numerical Examples

In this section, four examples are investigated. Far fields are compared with the Mie series [12] or VIE solution [14]. Surface currents of the first and last examples are also shown.

A. A Thin Dielectric Shell

A dielectric shell with radius 1.0 m, thickness 0.05 m, and dielectric constant 2.6 is examined. It is illuminated by a 0.2 GHz vertically polarized incident wave from $(\theta, \phi) = (180^0, 0^0)$. The sphere is modelled by 1,356 triangles. Fig. (3a) and (b) show the RCS at $\phi = 0^0$ and $\phi = 90^0$, respectively. For low contrast problem, apparently, it is not accurate enough by using

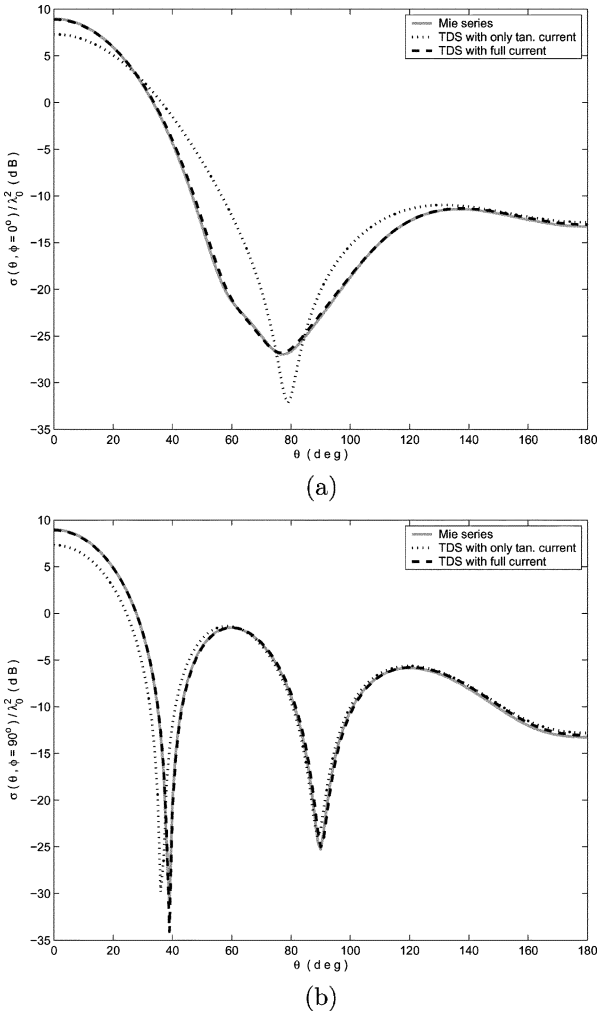

Fig. 3. Scattering by a dielectric shell with radius 1.0 m, thickness 0.05 m, $\varepsilon_r = 2.6$, and a vertically polarized incident wave from $(\theta, \phi) = (180^0, 0^0)$ at 0.2 GHz. (a) RCS at $\phi = 0^0$. (b) RCS at $\phi = 90^0$.

only tangential current proposed by [4] (dotted lines) since the normal current for small dielectric constant is comparable to the tangential component. To agree with the Mie series solution (solid lines), it is necessary to obtain both tangential and normal currents by our proposed method (dashed lines). Fig. 3(c), (d), and (e) show the tangential, normal, and full currents, respectively. The surface current (polarization current multiplied by the thickness) plot provides alternative check for the solution. It is interesting to note that tangential and normal currents are almost induced only by tangential and normal components of the incident fields, respectively. In other words, TM (normal current) and TE (tangential current) waves, with respect to the normal direction of a TDS, are almost decoupled locally in the thin dielectric layer since $\partial/\partial n \approx 0$ [20]. This implies that Z_{TN} and Z_{NT} in (17) are very small compared to Z_{TT} and Z_{NN}. A further check on matrix elements confirms this argument. In this case, it is more efficient to solve I_T and I_N in (17) separately.

B. A Thin Dielectric Strip

In this example, a $0.5\text{m}\times0.02\text{m}\times0.001\text{m}$ (in x, y and z dimensions, respectively) thin dielectric strip with $\varepsilon_r = 2.6$ at $z = 0$ is

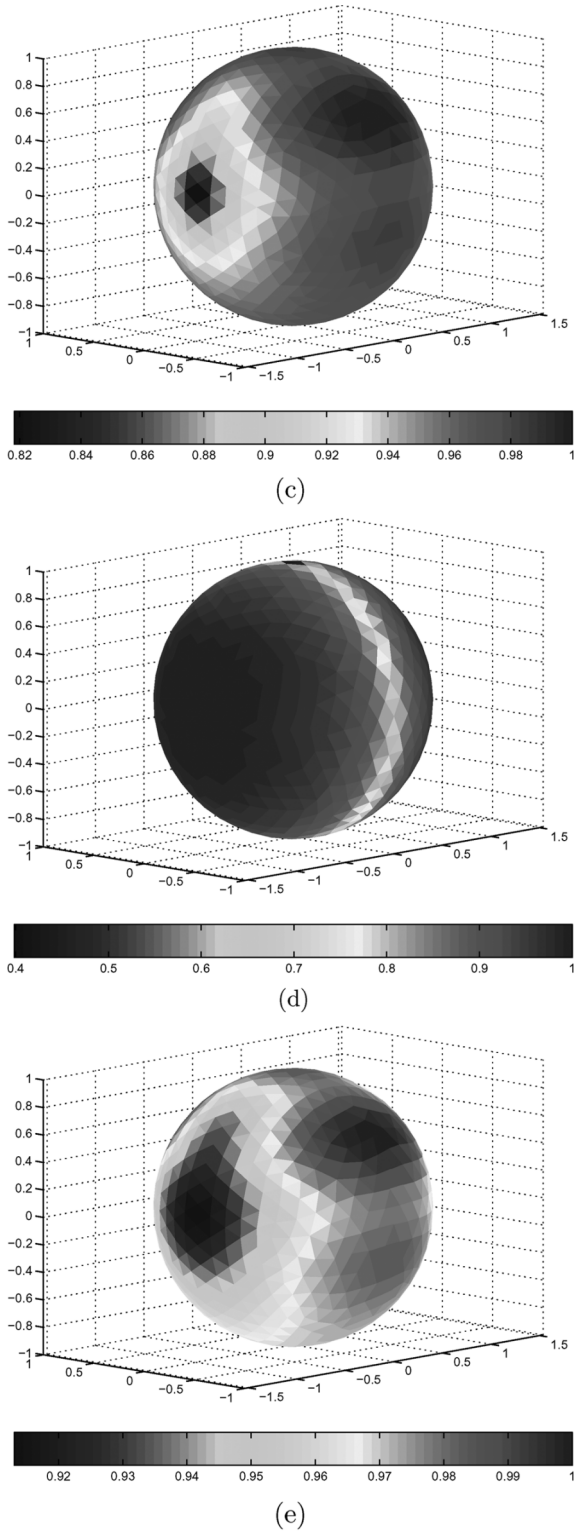

Fig. 3. (*Continued.*) Scattering by a dielectric shell with radius 1.0 m, thickness 0.05 m, $\varepsilon_r = 2.6$, and a vertically polarized incident wave from $(\theta, \phi) = (180^0, 0^0)$ at 0.2 GHz. (c) Tangential current. (d) Normal current. (e) Full current.

illuminated by a 0.2 GHz incident wave from $(\theta, \phi) = (180^0, 0^0)$. It is modelled by 452 triangles for TDS SIE and 1,408 tetrahedrons for VIE. Fig. 4 shows the RCS at $\phi = 0^0$ by a horizontally polarized illumination while Fig. 5 shows the RCS at $\phi = 0^0$ by a vertically polarized illumination. The difference of the RCS by

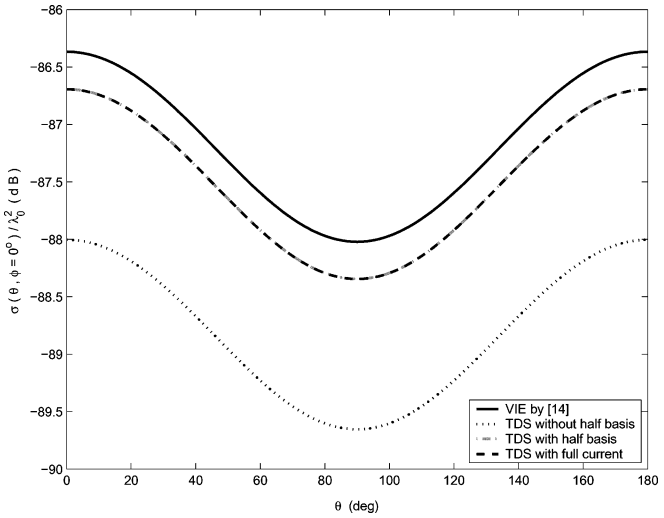

Fig. 4. RCS at $\phi = 0^0$ of scattering by a dielectric strip with dimension $0.5\ \mathrm{m} \times 0.02\ \mathrm{m} \times 0.001\ \mathrm{m}$, $\varepsilon_r = 2.6$, and a horizontally polarized incident wave from $(\theta, \phi) = (180^0, 0^0)$ at 0.2 GHz.

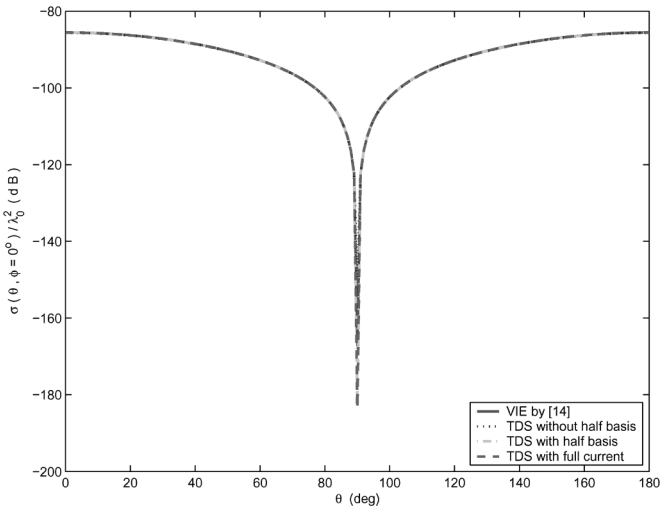

Fig. 5. RCS at $\phi = 0^0$ of scattering by a dielectric strip with dimension $0.5\ \mathrm{m} \times 0.02\ \mathrm{m} \times 0.001\ \mathrm{m}$, $\varepsilon_r = 2.6$, and a vertically polarized incident wave from $(\theta, \phi) = (180^0, 0^0)$ at 0.2 GHz.

the method with half basis functions (dashed lines) and VIE (solid lines) is less than 0.4 dB and 0.03 dB for horizontal and vertical excitations, respectively. The larger discrepancy for the horizontal case may come from the inaccurate evaluation of edge charge. However, the difference of the RCS by the method without half basis functions (dotted lines) and VIE is 1.7 and 0.08 dB for horizontal and vertical excitations, respectively. Since the horizontal case loses more y-direction current due to the inadequate RWG modelling, it gives a large deviation and a smaller RCS. Although this improper modelling also exists for the vertical case, the x-direction current is only a tiny portion of it. Therefore, it shows very good correspondence with VIE. On the whole, the modified RWG basis behaves more physically than the conventional RWG basis and thus gives more accurate results. The dashed-dotted lines in Figs. 4 and 5 are results by both tangential with half basis functions and normal currents. Since the normal current is tiny compared to the tangential current, the results are almost the same as those without it.

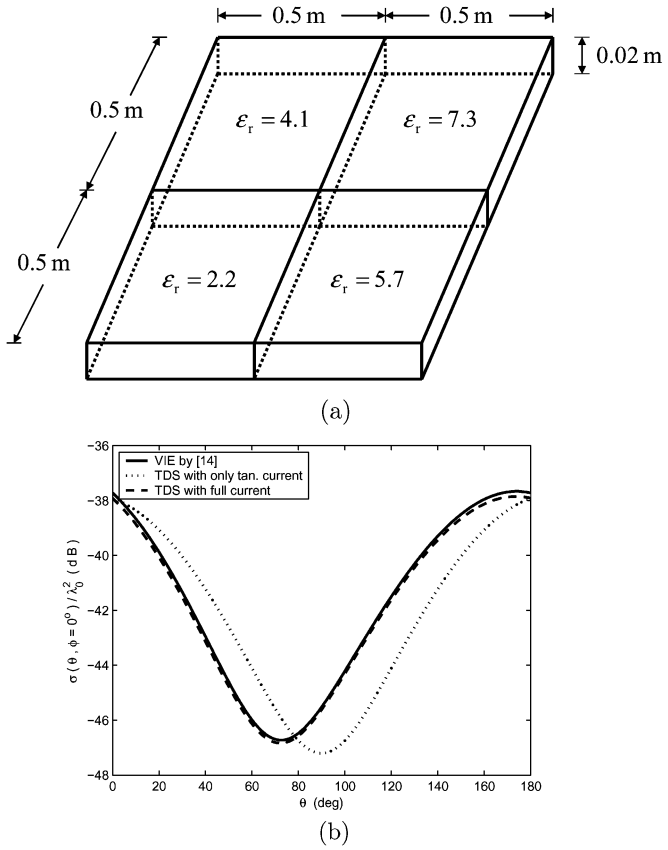

Fig. 6. Scattering by a $1.0\ \mathrm{m} \times 1.0\ \mathrm{m} \times 0.02\ \mathrm{m}$ inhomogeneous dielectric plate with $\varepsilon_r = 2.2$, 5.7, 4.1, and 7.3. The frequency is at 0.1 GHz and the incident wave is vertically polarized from $(\theta, \phi) = (120^0, 30^0)$. (a) The geometry. (b) RCS at $\phi = 0^0$.

C. An Inhomogeneous Thin Dielectric Square Plate

A $1.0\ \mathrm{m} \times 1.0\ \mathrm{m} \times 0.02\ \mathrm{m}$ inhomogeneous dielectric plate with $\varepsilon_r = 2.2$, 5.7, 4.1, and 7.3 is located at $z = 0$ and is illuminated by a vertically polarized incident wave from $(\theta, \phi) = (120^0, 30^0)$ at 0.1 GHz. Fig. 6(a) shows the geometry and Fig. 6(b) shows the RCS by VIE (solid line) modelled using 1,259 tetrahedrons, TDS using only tangential current with half basis (dotted line), and TDS using full current (dashed line). The TDS is modelled by 544 triangles. The result by full current TDS formulation has good agreement with that by VIE. The capability of handling inhomogeneity by (13) with modified RWG and pulse basis is also confirmed.

D. A Thin-Wall Radome

In the last example, we employ a thin-wall radome for testing our method. The radome is with thickness 0.002 m and dielectric constant 2.6 and is illuminated by a vertically polarized incident wave from $(\theta, \phi) = (120^0, 30^0)$ at 2.345 GHz. The RCS, tangential current, normal current and full current are shown in Fig. 7. It can be seen in Fig. 7(a) that the result by our new TDS formulation with full current (dashed line), modelled by 417 triangles, agrees excellently with that by VIE (solid line), modelled by 1,251 tetrahedrons. The result with only tangential current (dotted line) is also plotted for comparison. This radome

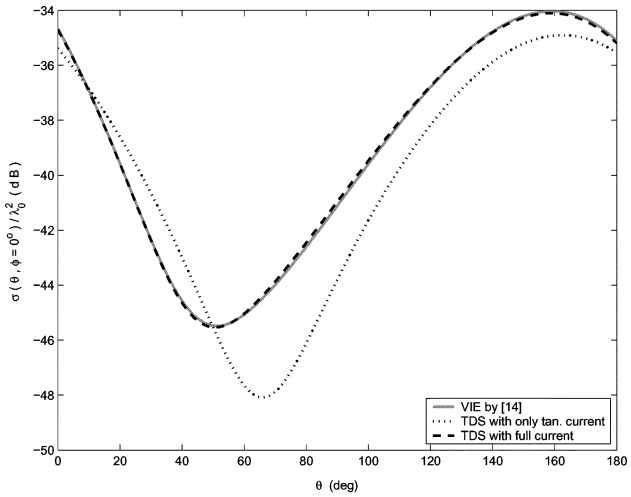

(a)

Fig. 7. Scattering by a radome with thickness 0.002 m, $\epsilon_r = 2.6$, and a vertically polarized incident wave from $(\theta, \phi) = (120^0, 30^0)$ at 2.345 GHz. (a) RCS at $\phi = 0^0$.

is modelled according to the radome for a modern mobile antenna. The agreement between our method and VIE shows the capability of handling practical complex geometry.

VI. Conclusion

We have reviewed the conventional TDS formulation. The validity and applicability of using this TDS approximation have been discussed as well. A new TDS formulation has been proposed where both tangential and normal currents are included. This new TDS SIE extends the capability to handle low dielectric constant, inhomogeneous and grazing incident problems. For thin sheet problems, the TDS SIE is more efficient than VIE to solve. Typically, it only needs one-third unknown count of the VIE approach using tetrahedral modelling. However, the RWG basis should be modified to include half basis functions so that anomalies do not happen in some special situations. This new method has been verified by Mie series and VIE considering inhomogeneity, media contrast, polarization, incident direction, and geometrical complexity and shows excellent agreement with them.

For scattering or radiation problems, a TDS is usually coated on the metal, sandwiches the frequency-selective surface or encloses an antenna. For circuit problems, layer structure is used extensively in modern circuit board. Hence, a hybrid TDS-PEC problem is of practical interest to solve. This task is currently in progress and it will be soon reported.

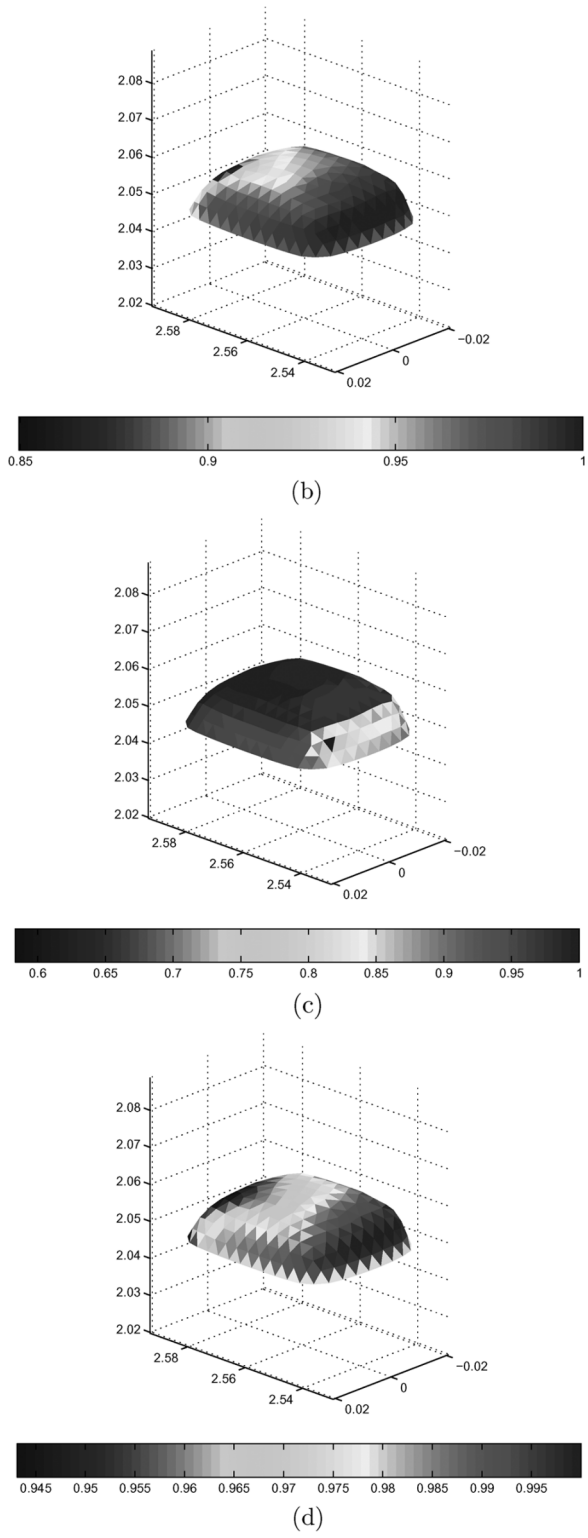

(b) (c) (d)

Fig. 7. (*Continued.*) Scattering by a radome with thickness 0.002 m, $\epsilon_r = 2.6$, and a vertically polarized incident wave from $(\theta, \phi) = (120^0, 30^0)$ at 2.345 GHz. (b) Tangential current. (c) Normal current. (d) Full current.

References

[1] J. D. Walton, Jr, Ed., *Radome Engineering Handbook: Design and Principles*. New York: Marcel Dekker, 1970.

[2] L. A. Pilato and M. J. Michno, *Advanced Composite Materials*. Berlin: Springer-Verlag, 1994.

[3] A. Baker, S. Dutton, and D. Kelly, Eds., *Composite Materials for Aircraft Structures*, 2nd ed. Reston, VA: AIAA, 2004.

[4] R. F. Harrington and J. R. Mautz, "An impedance sheet approximation for thin dielectric shells," *IEEE Trans. Antennas Propag.*, vol. AP-23, pp. 531–534, Jul. 1975.

[5] E. H. Newman and M. R. Schrote, "An open surface integral formulation for electromagnetic scattering by material plates," *IEEE Trans. Antennas Propag.*, vol. AP-32, pp. 672–678, Jul. 1984.

[6] T. B. A. Senior, "Combined resistive and conductive sheets," *IEEE Trans. Antennas Propag.*, vol. AP-33, pp. 577–579, May 1985.

[7] T. B. A. Senior and J. L. Volakis, "Sheet simulation of a thin dielectric layer," *Radio Sci.*, vol. 22, pp. 1261–1272, Dec. 1987.
[8] E. Arvas and S. Ponnapalli, "Scattering cross section of a small radome of arbitrary shape," *IEEE Trans. Antennas Propag.*, vol. 37, pp. 655–658, May 1989.
[9] E. Bleszynski, M. Bleszynski, and T. Jaroszewicz, "Surface-integral equations for electromagnetic scattering from impenetrable and penetrable sheets," *IEEE Antennas Propag. Mag.*, vol. 35, pp. 14–25, Dec. 1993.
[10] C. C. Lu, "A fast algorithm based on volume integral equation for analysis of arbitrarily shaped dielectric radomes," *IEEE Trans. Antennas Propag.*, vol. 51, pp. 606–612, Mar. 2003.
[11] W.-J. Zhao, L.-W. Li, and Y.-B. Gan, "Efficient analysis of antenna radiation in the presence of airborne dielectric radomes of arbitrary shapes," *IEEE Trans. Antennas Propag.*, vol. 53, pp. 442–449, Jan. 2005.
[12] R. F. Harrington, *Time-Harmonic Electromagnetic Fields*. New York: IEEE Press, 2001.
[13] D. E. Livesay and K. M. Chen, "Electromagnetic fields induced inside arbitrarily shaped biological bodies," *IEEE Trans. Microwave Theory Tech.*, vol. MTT-22, pp. 1273–1280, Dec. 1974.
[14] D. H. Schaubert, D. R. Wilton, and A. W. Glisson, "A tetrahedral modeling method for electromagnetic scattering by arbitrarily shaped inhomogeneous dielectric bodies," *IEEE Trans. Antennas Propag.*, vol. AP-32, pp. 77–85, Jan. 1984.
[15] C. Y. Shen, K. J. Glover, M. I. Sancer, and A. D. Varvatsis, "The discrete Fourier transform method of solving differential-integral equations in scattering theory," *IEEE Trans. Antennas Propag.*, vol. 37, pp. 1032–1041, Aug. 1989.
[16] P. Zwamborn and P. M. van den Berg, "The three dimensional weak form of the conjugate gradient FFT method for solving scattering problems," *IEEE Trans. Antennas Propag.*, vol. 40, pp. 1757–1766, Sep. 1992.
[17] R. F. Harrington, *Field Computation by Moment Methods*. New York: IEEE Press, 1993.
[18] S. M. Rao, D. R. Wilton, and A. W. Glisson, "Electromagnetic scattering by surfaces of arbitrary shape," *IEEE Trans. Antennas Propag.*, vol. AP-30, pp. 409–418, May 1982.
[19] H. Gan and W. C. Chew, "A discrete BCG-FFT algorithm for solving 3D inhomogeneous scatterer problems," *J. Electromag. Waves. Appl.*, vol. 9, pp. 1339–1357, 1995.
[20] W. C. Chew, *Waves and Fields in Inhomogeneous Media*. New York: Van Nostrand Reinhold, 1990, reprinted by IEEE Press, 1995.

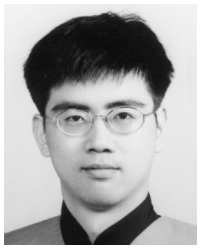

I-Ting Chiang (S'02–M'03) was born in Taichung, Taiwan, in 1973. He received the B.S., M.S., and Ph.D. degrees in electrical engineering from National Taiwan University, Taipei, Taiwan, R.O.C., in 1996, 1998, and 2002, respectively.

Since October, 2002, he has been with the Center for Computational Electromagnetics and Electromagnetics Laboratory (CCEML), Department of Electrical and Computer Engineering, University of Illinois at Urbana-Champaign, as a Postdoctoral Research Associate. His areas of interest include computational electromagnetics (CEM), thin sheet analysis, low-frequency electromagnetics, and fast algorithms for integral equations and nonlinear circuits.

Weng Cho Chew (S'79–M'80–SM'86–F'93) was born in Malaysia, on June 9, 1953. He received the B.E., M.S., Engineer, and Ph.D. degrees, all in electrical engineering, from the Massachusetts Institute of Technology, Cambridge, in 1976, 1978, 1978, and 1980, respectively.

Previously, he was a Department Manager and a Program Leader at Schlumberger-Doll Research, Ridgefield, CT. Currently, he is a Professor at the University of Illinois at Urbana-Champaign, where he is also the Director of the Center for Computational Electromagnetics and the Electromagnetics Laboratory. His research interest is in the area of waves in inhomogeneous media for various sensing applications, integrated circuits, microstrip antenna applications, and fast algorithms for solving wave scattering and radiation problems. He is the originator several fast algorithms for solving electromagnetics scattering and inverse problems. He has lead a research group that has developed parallel codes that solve tens of millions of unknowns for integral equations of scattering. He authored *Waves and Fields in Inhomogeneous Media* (New York: Van Vostrand Reinhold, 1990: reprinted by Piscataway, NJ: IEEE Press, 1995), coauthored *Fast and Efficient Methods in Computational Electromagnetics* (Norwood, MA: Artech House, 2001), and authored and coauthored over 300 journal publications, over 400 conference publications, and over ten book chapters.

Dr. Chew is an OSA Fellow, an IOP Fellow, and was an NSF Presidential Young Investigator. He received the Schelkunoff Best Paper Award for the IEEE TRANSACTIONS ON ANTENNAS AND PROPAGATION, the IEEE Graduate Teaching Award, Campus Wide Teaching Award, and was a Founder Professor of the College of Engineering, and currently, a Y. T. Lo Endowed Chair Professor in the Department of Electrical and Computer Engineering at the University of Illinois. Since 2005, he serves as an IEEE Distinguished Lecturer. Recently, ISI Citation elected him to the category of *Most-Highly Cited Authors* (top 0.5%) He served on the IEEE Adcom for Antennas and Propagation Society as well as Geoscience and Remote Sensing Society. He has been active with various journals and societies.